MET O 19 BRANCH MEMORANDUM NO 79

REMOVAL OF CLOUD CONTAMINATION FROM AVHRR INFRARED RADIANCES

by

R.W.SAUNDERS

January 1985

Met O 19 (Satellite Meteorology Branch)
Meteorological office
London Road
Bracknell
Berks RG12 2SZ

Removal of Cloud Contamination from AVHRR Infrared Radiances

1. Introduction

One of the major problems in satellite retrievals of surface parameters from infrared radiances is the correct identification and removal of cloud contamination. Typically 50% of the earth's surface is covered by cloud at any one time. Different types of cloud present different problems, for instance thin cirrus cloud cannot be detected easily at visible wavelengths. Low stratus and fog on the other hand are difficult to detect at infrared wavelengths over the sea surface because their temperatures are close to that of the underlying surface. The techniques discussed here aim to determine whether any cloud is contaminating an individual radiance (pixel) and hence to compute a mean cloudfree radiance or brightness temperature over the required area. Having obtained cloudfree brightness temperatures it is then proposed to use these to derive mean cloud parameters such as cloud fraction, cloud top height and optical depth. This two step process has also been adopted by the the International Satellite Cloud Climatology Project (ISCCP) (Schiffer and Rossow;1983, World Climate Programme;1984) for the computation of mean cloud parameters.

Cloud detection algorithms operate more successfully over a uniform surface of constant temperature and emissivity such as sea surface than over land where both quantities can vary in space and time. Whereas cloud analysis algorithms need only flag pixels >50% cloud covered as cloudy, algorithms for cloudfree brightness temperature retrievals should flag pixels >1% cloud covered as the cloud can still have a significant ($\sim$0.2K) effect on the measured brightness temperature. The measured radiance is a combination of the cloudfree surface radiance and cloud top radiance (usually colder than the surface) after transmission through the atmosphere. Neglecting atmospheric absorption/emission effects, cloud types of high optical thickness will modify the measured infrared IR radiance E according to the following expression:

$$E_{pix} = \int_{\nu_1}^{\nu_2} \left[\alpha \epsilon_{cl} B(\nu, T_{cl}) + (1-\alpha)\epsilon_s B(\nu, T_s) \right] \psi(\nu) d\nu \qquad (1)$$

where $B(\nu,T)$ is the Planck function; α is the fractional cloud amount within the pixel; ϵ is the effective emissivity; and $\psi(\nu)$ the normalised filter profile. ν_1 and ν_2 are the lower and upper frequency limits of the filter profile and the subscripts s and cl denote surface and cloud respectively.

The effect of different cloud fractions at different heights on the measured radiance computed using equation 1 is shown in figure 1a at 3.7μm (AVHRR channel 3) and in

figure 1b at 11μm (AVHRR channel 4). Emissivities of cloud tops and surface at the two wavelengths shown in figure 1 were taken from Hunt (1973). It is important to note that a change of cloud fraction from clear to only 10% with tops at 230K will alter the measured cloudfree brightness temperature by 4K at 11μm.

For high cold cloud tops (230K) the effect of increasing cloud cover at 3.7μm is less than at 11μm due to the greater sensitivity of the Planck function to temperature at 3.7μm. This has the interesting effect shown in figure 1c that the difference between the brightness temperatures in the two channels varies markedly with fractional cloud cover. The large values (~10K) of T3.7-T11 shown in figure 1c would also be obtained with a cloud of low optical depth and complete cloud cover. This temperature difference allows the optical depth of a cloud to be determined as shown by Olesen and Grassl (1984). Also evident in figure 1c is the effect reported by Eyre et al (1984) where for cloud filled pixels (ie a cloud fraction of 100%) the 11μm brightness temperature is greater than the 3.7μm brightness temperature due to the difference in cloud emissivity at the two wavelengths.

Although equation 1 neglects atmospheric absorption/emission effects which are appreciable at both 3.7 and 11μm, the results shown in figure 1 are not modified significantly when atmospheric absorption effects are included because attenuation due to clouds has a much greater effect than absorption due to atmospheric gases.

This paper compares the performance of five different cloud detection algorithms for daytime AVHRR scenes over the UK and western Europe. From this comparison an optimum automated scheme for obtaining cloudfree brightness temperatures over land and sea during the day is recommended.

2.Description of Different Cloud Detection Techniques

There are a number of different cloud detection techniques which have been developed by various groups to identify cloud contaminated radiances. The results described below compare a number of these and try to identify where problems can arise with each method.

2.1 Spatial Coherence Technique

The first method considered is a simplified version of the spatial coherence technique developed by Coakley and Bretherton (1982) which relies on the fact that cloud top radiances normally vary over small space scales whereas the radiance from the sea surface is uniform. This method has an important advantage that only infrared radiances are required (normally at a wavelength of 11μm) so the same

procedure can be used day and night. The method consists of defining a small 'local' array (in this case chosen to be 3 x 3 AVHRR 1.1 km pixels) and calculating local means T and standard deviations SD over each local array of brightness temperatures. First a gross cloud check is applied which rejects all arrays with local means less than a predefined brightness temperature (272K over sea and 260K over land) as cloud contaminated. A more sophisticated scheme could vary the land brightness temperature threshold depending on the time of day and season. Next all local arrays with standard deviations greater than a predetermined threshold value (0.2K over sea, 1.0K over land and coast) are also flagged as being cloud contaminated. Pixels which are not flagged will then contribute to the mean cloudfree brightness temperature for the area. The predetermined standard deviation thresholds listed in table 1 will depend on the small scale temperature variability of the underlying surface, the noise equivalent temperature of the radiometer and digitisation interval of the radiometer counts. This method does not work as well over land (or over strong horizontal gradients in sea surface temperature) because the surface radiance is not uniform and could be incorrectly identified as cloud. For this reason the standard deviation threshold value is increased over land and coastal regions to allow for the surface variability in brightness temperature even though this may allow some cloudy pixels to escape detection.

2.2 Dynamic Visible Threshold Technique

A technique commonly used during the day is to use solar reflected and scattered radiances at visible and near infrared wavelengths to detect cloud. Most cloud types have a high reflectance at these wavelengths when compared with the low reflectance of the sea surface away from areas of specular reflection. This allows a visible threshold to be applied where all reflected radiances above a certain level are identified as cloud contaminated. Longer wavelengths (ie 0.9μm AVHRR channel 2) are less affected by aerosols than at shorter wavelengths (ie 0.65μm AVHRR channel 1) but land surfaces have a higher albedo at longer wavelengths. This favours the use of the longer wavelengths for retrievals over the sea as radiances will not be affected as much by scattering. Also any land in the field of view will have high radiance and be flagged as cloudy not contributing to the mean sea surface temperature (SST). Shorter wavelengths are more useful over land as it has a much lower reflectance at 0.65μm than at 0.9μm making the contrast between the land and cloud much greater and hence detection of cloud easier. For both channels the threshold is 'dynamically' determined from the histogram of all the visible radiances over the region of interest. In figure 2a a typical visible radiance histogram with a cloudfree peak is shown together with the various parameters used to compute the threshold value. First the peak radiance Ipk and number of radiances that make up the histogram peak

value (ie population) are determined and if it is significant (ie contains more than 0.5% of the total population) the process continues. The lower I1 and upper I2 limits of the histogram are then determined. If the low radiance end I1 of the histogram is within m counts of the histogram peak and the peak radiance is less than that over a typical cloud scene Imax then the peak is assumed cloudfree and the visible threshold T is set at n radiance counts above the peak radiance. The values for m,n and Imax over different surface types is given in table 1. These values were determined empirically for AVHRR data by looking at a number of histograms from different images at different times of the year. However a more sophisticated algorithm which varies these constants as a function of solar illumination would be desirable. If a cloudfree peak is not found in the histogram then all pixels are flagged as cloudy. Over coastal regions the visible histogram can have two cloudfree peaks as shown along the ordinate of figure 4d. In this case the dynamical threshold technique does not work successfully. Either the cloudfree sea peak alone is identified or the cloudfree land peak is incorrectly identified as cloud. To overcome this problem a straightforward constant threshold method is used in coastal areas which flags all pixels with a reflected radiance greater than Imax as cloud contaminated. This does mean however that low cloud over coastal regions can more easily escape detection. A major disadvantage of this visible threshold technique is that it can only be used during the day. In addition it cannot be used over sea in areas of sunglint.

2.3 Spatial Coherence Visible (SCV) Technique

The third algorithm used is a combination of the above two methods termed the Spatial Coherence Visible technique (SCV) as used successfully by Llewellyn Jones et al (1984) to compare satellite and ship SST's. Coakley and Baldwin (1984) also found that by making use of the visible channel in conjunction with the spatial coherence method improved their cloudfree brightness temperatures. The two methods, applied to a 50x50 pixel array, complement each other as the spatial coherence technique is good at detecting thin cirrus and insensitive to sunglint whereas the visible reflected radiances discriminate well between low cloud and sea surface and are not affected by strong temperature gradients near SST frontal regions. In areas of sunglint or at night only the spatial coherence method is used. A schematic flow chart of this algorithm is shown in figure 3.

2.4 Bispectral Technique

The fourth method is a bispectral technique where both visible radiance (channel 1 or channel 2) and brightness temperature (channel 4) histograms of each area are analysed to determine cloudfree brightness temperatures. Figure 4

shows some examples of bidimensional histograms of 50x50 pixel areas for visible radiances (channel 1 over land or channel 2 over sea) and infrared (channel 4) brightness temperatures. In figure 4a a dark, warm peak is seen corresponding to cloudfree sea radiances. Cloud contaminated pixels are displaced from this peak when stratocumulus and cirrus clouds enter the fields of view. Their distance from the cloudfree peak is dependent on the fractional cloud cover within the pixel, cloud optical depth and differences between the cloud top and surface brightness temperatures and reflectances. The angle which the cloud contaminated pixels are offset from the cloudfree peak is a function of the brightness temperature and reflectivity differences between the cloud top and surface. For instance in figure 4a the cloud contaminated pixels lie at different angles to the peak due to both cirrus and low stratocumulus contaminating the pixels. The cirrus contaminated pixels are at 30 degrees (to the abscissa) from the cloudfree peak whereas the stratocumulus contaminated pixels are at 60 degrees. Over land the cloudfree peak is much broader due to the greater variability of surface temperature and reflectance. Figure 4b shows peaks in both histograms corresponding to cloudfree radiances over land. Thin cirrus was present which modifies the channel 4 radiance histogram but channel 1 radiances remained unaffected by thin cirrus. Figure 4c shows the effect a cumulus cloud field has on the radiances over land. Again both histograms have a broad cloudfree peak but cloud contaminated pixels broaden the bright and cold ends of the channel 1 and channel 4 radiance histograms respectively.

The brightness temperature and visible radiance histograms are analysed in the same way as the visible threshold technique described above by 'dynamically' computing a cloudfree threshold value in both channels as shown in figure 2a and 2b. When computing the infrared threshold the difference between the peak and the high radiance end I2 of the histogram is used to ascertain whether the peak is due to cloudfree radiances or not. If a cloudfree peak is not found in either the infrared or visible histogram then all pixels are flagged as cloudy. The constants used are listed in table 1. In an operational system a better and computationally faster solution may be to use the last cloudfree radiances derived over this area to define rough threshold values. This would work well over the sea where the surface temperature and reflectivity remain relatively constant from day to day.

Figure 4d shows the histograms in a cloudfree coastal area where there are two distinct cloudfree peaks in each histogram. This prevents the use of simple dynamical thresholding techniques as already described above for the visible threshold method.

2.5 Cloud Detection Using 3.7um Radiances

The final method makes use of radiances from the 3.7μm channel to detect cloud. The use of this channel at night has already been considered (Eyre et al;1984 and Olesen and Grassl;1984). The appearance of a night 3.7μm image is similar to the corresponding 11μm image. However the emissivity of cloud or fog at 3.7μm can be significantly less than at 11μm (Hunt;1973) producing a measurable difference in measured brightness temperature between the two channels much greater than the differences caused by atmospheric absorption at midlatitudes. This emissivity difference has been successfully exploited (Eyre et al;1984) to demonstrate how fog can be detected at night by measuring the difference in brightness temperatures between the two channels. This is important since low cloud at night is the most difficult cloud to detect with either IR threshold or spatial coherence methods.

During the day the 3.7μm radiance consists of not only emitted terrestrial radiation but also reflected solar radiation from surfaces and clouds with high reflectivities at these wavelengths. This can lead to an image of complex appearance with clouds of low radiance such as cirrus (low reflectivity and low brightness temperature) and clouds of high radiance such as cumulus clouds (high reflectivity and high brightness temperature). The low clouds with high reflectivities at 3.7μm can be detected in the same way as for the visible channel. To compare the visible and 3.7μm reflected radiances over low cloud and cloudfree sea surface figure 5 was plotted which is a bidimensional histogram of NOAA 6 AVHRR radiances from channels 2 and 3. Both histograms are of the original radiances received by the satellite and not enhanced in any way. It is clear that the 3.7μm (channel 3) radiances are more sensitive to the presence of the stratocumulus cloud than the visible (channel 2) radiances. This suggests that 3.7μm radiances may in fact be better than visible reflected radiances for the detection of low cloud during the day. However clouds with higher reflectivities and lower brightness temperatures can have the same radiance as the cloudfree sea surface so a simple threshold method will not work in this case. These clouds of lower brightness temperature should be detectable with the 11μm infrared channel so a histogram of only 3.7μm radiances with brightness temperatures > 250K at 11μm is computed. Then using the 'dynamical' threshold technique described above on this histogram and the constants given in table 1 a cloudfree peak is identified and a threshold value can be set which discriminates between cloud and cloudfree areas. This method may not cope with all cloudy radiances as reflected and emitted radiation at 3.7μm also depends on the microphysical parameters of the cloud such as drop size and water/ice phase (Arking and Childs;1983). In common with the visible channels cloud detection is more difficult in areas of sunglint.

Another possibility is to use the 3.7μm radiance in a spatial coherence scheme as described above for the 11μm radiances. This may be a more effective way of using 3.7μm radiances to detect cloud. However the spatial coherence method is sensitive to the noise level of the individual radiances making this possibility impractical with noise levels currently obtained with the AVHRR channel 3 instrument (ie TIROS-N to NOAA 8).

3.Comparison of Results

The five different algorithms described above were all tested on 1.1km AVHRR/2 local area coverage (LAC) data recorded over the British Isles for two days, 16 July 1983 at 1426 GMT and 5 March 1982 at 1337 GMT. The data were obtained from the University of Dundee receiving station. The algorithms were applied over 50 x 50 pixel arrays with a mean cloudfree brightness temperature being computed for each array.

The results from the first four methods over different cloud and surface types are shown in table 2 for 16 July 1983, where the numbers along the top and side define the box coordinates (x,y). The corresponding visible (channel 2) image for this area is shown in figure 6 with boxes overlayed. A value of -1 indicates that all pixels in the box are identified to be cloud contaminated so no cloudfree brightness temperatures could be computed. The 3.7μm radiances were too noisy at this time to allow radiances from this channel to be used.

Comparing the four different methods there are a number of discrepancies evident. In box (3,4) for instance cirrus cloud was present, which has not been detected by the visible threshold method giving an unrealistic low temperature. The other three methods detect the cirrus successfully in this box. However in the adjacent box (4,4) the spatial coherence method has also identified a region of uniform IR radiance giving a bad temperature value which also appears in the SCV value. Another problem which is demonstrated in box (11,2) and surrounding boxes is the failure of the spatial coherence method to detect a uniform stratus cloud top layer whereas the visible threshold method successfully rejects all radiances as cloud contaminated. The temperature of the stratus cloud top in this case was about 5 degrees lower than the surrounding sea surface so this could have been filtered out if a background brightness temperature is known. In box (4,10) which is a coastal area both spatial coherence and simple visible threshold methods have not completely identified all of the cirrus cloud present resulting in an erroneously low cloudfree brightness temperature for this box. In boxes (6,10) to (12,10) (along the south coast) the bispectral method has failed each time. This is due to small areas of warm land present in the box which in the histogram makes the difference between the

maximum radiance and cloudfree peak radiance m greater than the 100 counts maximum given in table 1.

The SCV method and bispectral analysis agree in most boxes but there are one or two interesting differences. A limitation of the bispectral technique over the sea is in boxes where a strong SST gradient exists (eg box (1,6)). In these cases the cloudfree IR histogram will have two peaks corresponding to the warm water and cold water temperatures. This will cause problems for the histogram analysis possibly rejecting the cold water radiances as cloud contaminated and giving a warm bias to the SST. The SCV method on the other hand will reject the pixels over the actual SST front as cloudy because of the large local standard deviation in surface radiance but will retain the uniform warm and cold areas as cloudfree to give a more representative mean value. Over land (eg around box (9,8)) the SCV method gives a consistently lower surface brightness temperature than the bispectral analysis due to the variability in the surface temperature as for the sea case described above. In apparently cloudfree areas (eg box(9,9)) shown in figure 6 the difference of typically 1K still exists suggesting that it is not caused by undetected clouds by the SCV method but by the bispectral technique giving the maximum cloudfree brightness temperature rather than the mean.

The second dataset for 5 March 1982 was chosen to allow the 3.7μm cloud detection algorithm to be included as at this time the noise level was low for NOAA 7 AVHRR channel 3. Figure 7 shows a comparison between the cloudfree brightness temperatures computed by the SCV method (using channel 2 over the sea and channel 1 over the land) and the algorithm using 3.7μm radiances instead of the visible channels. Over the sea the agreement is good (~0.1K) suggesting in this case that either algorithm could be used. Over the land however the contrast between the surface and low cloud at 3.7μm radiances is small making cloud detection more difficult with the algorithm failing in some cases.

4.Discussion

The comparison of the results from the different algorithms shown in table 2 and figure 6 suggests that the SCV method in most cases performs better than the others as long as the constants are changed according to the underlying surface as shown in table 1. The principal advantage of this method over the bispectral analysis technique is shown best where there is an abrupt change in the surface temperature within the box. Under these conditions the SCV method will give a more representative mean cloudfree brightness temperature whereas the bispectral analysis will tend to give the maximum temperature. Also in coastal areas the SCV method manages to retrieve a cloudfree brightness temperature more often than the bispectral analysis as the latter method does not work well with two

cloudfree peaks in the histogram. The algorithm using 3.7μm radiances in place of visible radiances appears to work as well over sea areas and the evidence of figure 5 suggests for certain cloud types (eg Sc) cloud detection at these wavelengths may be better. To demonstrate the success of the SCV method figure 6 shows retrieved cloudfree brightness temperature using this method for 16 July 1983 from table 2, over the corresponding visible (AVHRR channel 2) image. The number of cloudfree pixels computed by the algorithm is also given showing the number of pixels which passed all the tests in the SCV algorithm. If a background field of cloudfree brightness temperature from previous days satellite observations or from surface reports had been available many of the anomalous values computed could have been filtered out. This additional improvement is easy to include in an operational scheme but difficult to set up for individual case studies such as reported here.

On a VAX 11/750 the SCV method took approximately 1.1secs for one 50 x 50 pixel box with the spatial coherence part taking 0.25secs and the dynamic visible threshold 0.85secs. The bispectral analysis took 1.7secs and the algorithm using the 3.7μm radiances 1.8secs. The coding of the algorithms was not optimised so an improvement on these times should be possible in an operational scheme.

As far as validation of these cloudfree brightness temperatures is concerned the simplest possibility is to compare SST values (computed using the cloudfree brightness temperatures with a multichannel regression relation such as that given in Llewellyn Jones et al (1984)) with good ship measurements. This was done in Llewellyn Jones et al (1984) using the SCV method described above giving root mean square differences of 0.6K between the ship and satellite measurements. Validation over land would be more difficult as the surface skin temperature can be as much as 10 degrees different from the screen temperature (Price;1984). A detailed comparison of surface skin temperatures measured from the ground and from a satellite would need to be performed to validate the removal of cloud contamination over land.

5.Conclusions

A comparison of the results from five cloud detection schemes over the UK and surrounding sea areas suggests that the spatial coherence visible (SCV) scheme is the most successful during the day. The cloudfree brightness temperatures obtained over the ocean using this method have been shown by Llewellyn Jones et al (1984) to give good agreement (0.6K) when compared with coincident ship measurements. Over land and coastal areas the standard deviation will be larger (~2K) due to the greater variability of the surface radiance making the algorithm thresholds less discriminating. Uniform thin cirrus proves

especially difficult to detect and is the main weakness of the SCV method. One way of improving the detection of thin cirrus would be to look at the difference between the 3.7 and 11μm brightness temperatures which will be sensitive to the presence of optically thin clouds as illustrated in figure 1c. A similar scheme using spatial coherence and 11μm/3.7μm brightness temperature differences will be developed for effective cloud detection at night.

6.References

Arking,A. and Childs,J.D. 1983 Extraction of cloud cover parameters from multispectral satellite measurements. Rep on 5th Conference on Atmospheric Radiation Oct 31 - Nov 4 1983 Baltimore MD. p 258-263

Coakley,J.A. and Bretherton,F.P 1982 Cloud cover from high resolution scanner data:detecting and allowing for partially filled fields of view J.G.Res 87,C7, p 4917-4932

Coakley,J.A. and Baldwin,D.G. 1984 Towards an objective analysis of clouds from satellite imagery data. J.C.A.M. 23 p 1065-1099

Eyre,J.R.,Brownscombe,J.L and Allam,R.J 1984 Detection of fog at night using Advanced Very High Resolution Radiometer (AVHRR) imagery. Met Mag. 113 p 266-271

Hunt,G.E. 1973 Radiative properties of terrestrial clouds at visible and infrared thermal window wavelengths. Q.J.R.Meteorol Soc 99 p 346-369

Llewellyn-Jones,D.T.,Minnett,P.J Saunders,R.W and Zavody,A.M. 1984 Satellite multichannel infrared measurements of sea surface temperature of the N.E.Atlantic Ocean using AVHRR/2. Q.J.R.Meteorol Soc 110 p 613-631

Olesen,F.S.and Grassl,H. 1984 Cloud detection and classification over oceans at night with NOAA 7. Intl J.of Remote Sensing (in print)

Price J.C. 1984 Land Surface Temperature Measurements from the split window channels of the NOAA 7

Advanced Very High Resolution Radiometer. J.G.Res 89 D5 p 7231-7237

Schiffer,R.A. and Rossow,W.B. 1983 The International Satellite Cloud Climatology Project (ISCCP).The first project of the World Climate Research Programme. Bull. Am. Met Soc 64 p 779-784

World Climate Programme 1984 Cloud Analysis Algorithm Intercomparison (ISCCP) WCP-73

Table 1: Algorithm Constants Used

Algorithm	Surface Type Sea	Land	Coast
Spatial Coherence			
Tmin	272K	260K	260K
Local SD Thresh	0.2K	1.0K	1.0K
Visible Histogram			
m	25	35	N/A
n	7	7	N/A
Imax	130	150	150
Infrared Histogram			
m	3.5K	12K	12K
n	0.8K	0.8K	0.8K
Tmin	272K	260K	260K
3.7μm Histogram	T11 > 250K		
m	25	50	50
n	7	7	7
Imax	900	900	900
Imin	750	750	750

The definitions of some of these constants are shown in figure 2. The visible and 3.7μm constants are in units of raw radiance as received from the spacecraft. The infrared constants are in units of brightness temperature.

Table 2: Comparison of Different Cloud Detection Algorithms

Box Coords	1	2	3	4	5	6	7	8	9	10	11	12
	10.0	15.6	18.9	17.1	11.3	13.1	14.9	15.2	7.7	6.8	4.1	3.3
1	-1.0	-1.0	19.9	17.3	11.4	13.5	15.4	18.1	-1.0	-1.0	-1.0	-1.0
	-1.0	-1.0	20.2	17.2	11.3	13.1	15.0	18.1	-1.0	-1.0	-1.0	-1.0
	-1.0	-1.0	-1.0	-1.0	-1.0	-1.0	-1.0	18.2	-1.0	-1.0	-1.0	-1.0
	17.3	17.2	12.5	12.5	11.9	13.3	15.6	13.9	11.3	9.4	8.2	7.2
2	20.0	19.5	14.1	12.5	12.8	13.7	15.8	20.5	-1.0	-1.0	-1.0	11.3
	19.7	19.5	14.1	12.4	12.6	13.5	15.6	20.7	-1.0	-1.0	-1.0	11.4
	20.0	19.5	13.9	12.6	12.0	12.5	14.5	-1.0	-1.0	-1.0	-1.0	-1.0
	12.0	15.5	10.6	11.3	11.8	12.9	15.8	19.2	17.3	10.4	10.2	10.0
3	-1.0	15.7	10.2	11.0	11.8	13.1	16.2	21.0	20.6	-1.0	-1.0	13.7
	-1.0	17.1	11.0	11.3	11.8	13.0	15.8	21.0	20.6	-1.0	-1.0	13.4
	-1.0	-1.0	-1.0	-1.0	-1.0	13.1	-1.0	22.8	20.7	-1.0	-1.0	-1.0
	11.1	2.1	-1.0	5.3	14.9	12.4	18.7	22.6	21.8	17.0	18.1	14.4
4	16.1	5.1	3.7	4.7	14.1	11.1	15.9	23.9	22.6	22.0	20.8	14.8
	17.5	5.7	-1.0	5.3	15.2	12.4	19.1	24.2	22.8	22.0	20.7	14.4
	-1.0	-1.0	-1.0	-1.0	-1.0	13.7	17.9	24.2	22.9	-1.0	21.0	-1.0
	14.1	11.6	12.1	8.1	5.8	25.3	17.3	21.4	19.4	20.6	20.2	15.9
5	14.1	11.5	12.0	8.1	13.2	24.6	-1.0	18.5	19.5	20.0	19.7	13.5
	14.1	11.6	12.2	11.2	14.9	25.4	-1.0	21.3	20.2	20.9	20.3	15.9
	-1.0	11.7	12.2	-1.0	-1.0	25.5	-1.0	19.8	22.2	22.0	21.2	17.1
	15.1	13.6	20.1	23.5	25.1	26.1	25.5	25.0	25.0	21.7	15.1	12.0
6	15.5	13.9	20.0	22.8	24.0	25.7	25.0	24.9	24.9	21.8	15.8	10.5
	16.0	13.6	20.1	24.0	25.5	26.3	26.0	25.2	25.2	23.0	18.8	13.8
	16.5	-1.0	-1.0	27.3	26.7	26.7	26.5	26.6	26.0	23.8	-1.0	-1.0
	17.1	14.9	15.6	20.8	26.6	26.2	26.4	26.2	23.4	24.5	19.7	17.4
7	16.9	13.8	15.5	20.4	26.6	25.6	25.3	25.8	22.7	23.9	23.3	16.8
	17.1	14.9	15.6	20.8	26.6	26.4	26.4	27.1	24.2	25.0	24.6	18.9
	17.1	16.4	-1.0	-1.0	27.5	26.9	26.7	27.4	24.3	26.2	25.7	18.8
	18.0	11.3	13.4	19.3	19.5	23.4	26.6	28.1	27.8	30.2	26.5	22.4
8	11.8	8.4	12.7	19.2	21.3	25.9	26.3	27.1	27.8	30.3	26.3	20.5
	18.0	11.8	13.4	19.3	20.0	26.2	27.0	28.1	28.4	30.5	26.6	22.4
	-1.0	15.1	-1.0	-1.0	-1.0	27.2	27.2	28.8	29.5	30.8	27.6	25.6
	15.1	11.2	15.2	21.5	25.2	26.2	25.4	27.6	28.2	29.3	29.0	21.5
9	15.8	11.2	14.3	15.0	18.0	26.1	25.0	26.1	25.7	28.4	28.7	22.7
	17.7	13.5	17.0	21.5	25.4	27.1	26.6	27.6	28.2	28.6	29.0	21.5
	-1.0	-1.0	-1.0	-1.0	-1.0	27.9	28.3	28.4	29.5	29.9	30.4	-1.0
	17.5	-1.0	-1.0	-0.2	11.5	14.8	15.6	17.1	17.9	20.2	21.9	18.1
10	15.8	-1.0	2.9	4.6	5.7	11.5	15.9	18.3	18.8	21.5	22.3	18.8
	17.5	-1.0	0.9	7.0	11.5	14.8	15.6	17.1	17.9	20.2	21.9	18.1
	-1.0	-1.0	-1.0	-1.0	-1.0	-1.0	-1.0	-1.0	-1.0	-1.0	-1.0	-1.0
	1	2	3	4	5	6	7	8	9	10	11	12

The cloudfree brightness temperatures are in degrees centigrade. They are derived over 50 x 50 pixel boxes. The four algorithms are from top to bottom spatial coherence technique, visible threshold method, SCV and bispectral analysis. A value of -1.0 indicates that the algorithm computed total cloud cover.

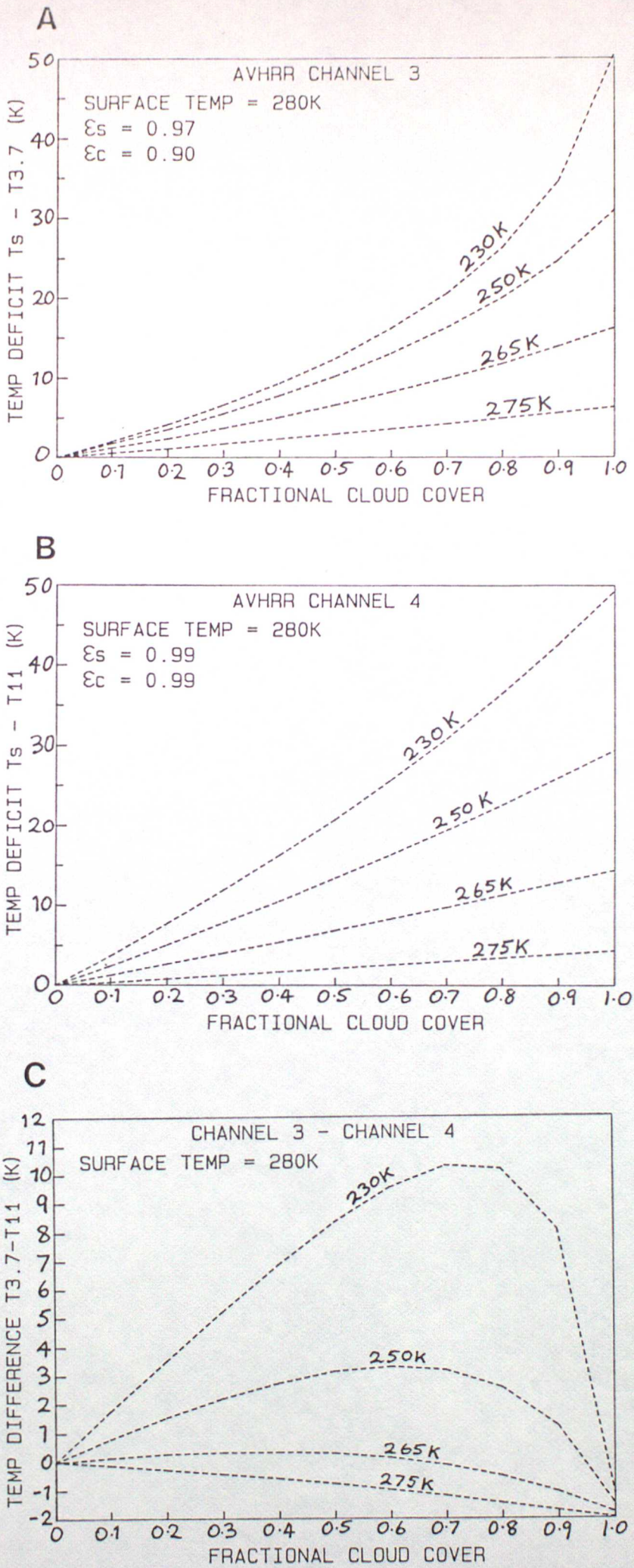

Figure 1. The effect of increasing the cloud amount on the radiances at (A) 3.7μm and (B) 11μm. Results for 4 different cloud top temperatures are shown assuming the surface and cloud emissivities listed. The difference between the brightness temperatures measured in the two channels is shown in (C).

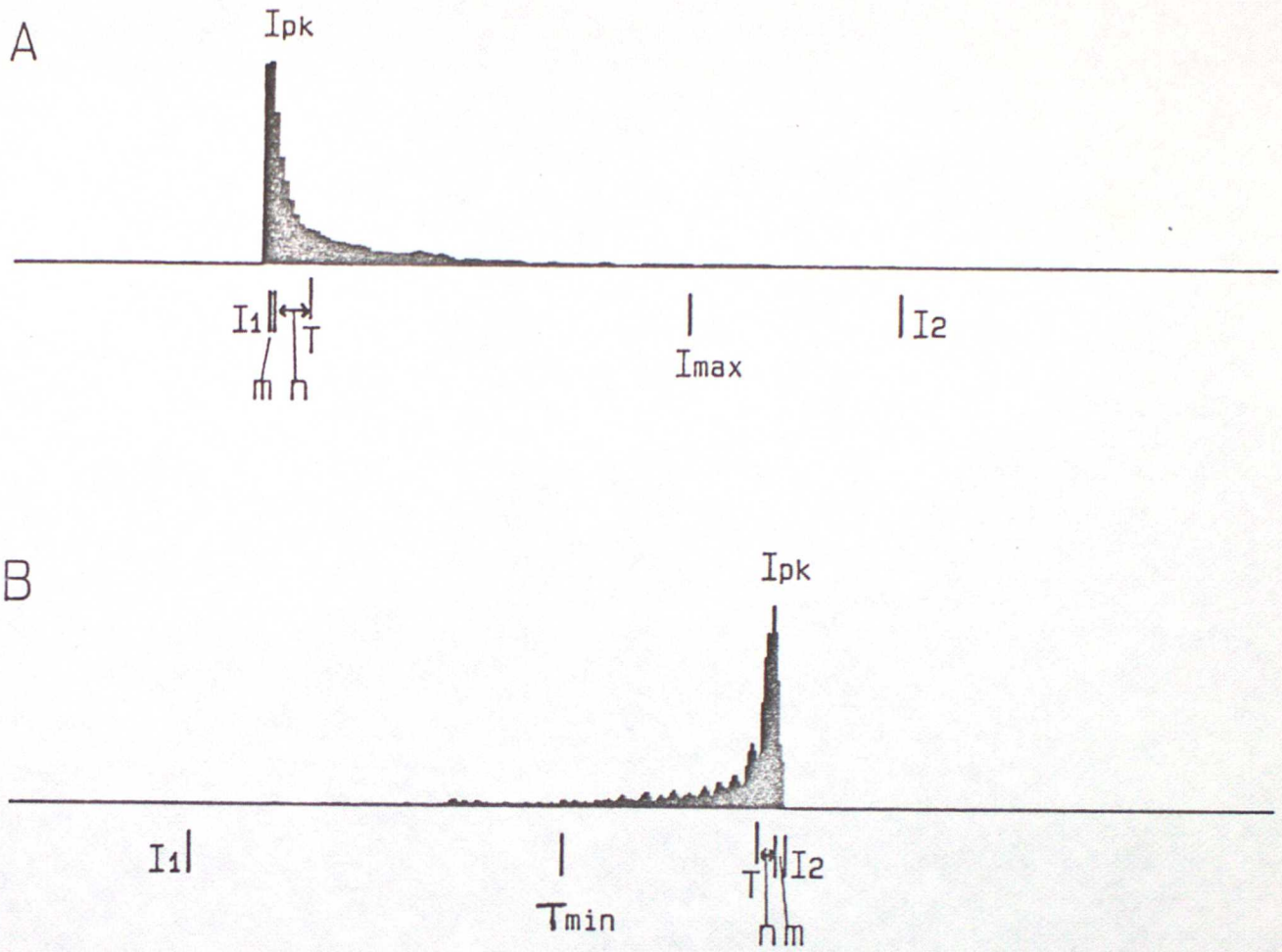

Figure 2. An example of visible radiance (A) and 11μm brightness temperature (B) histograms with cloudfree peaks. The 'dynamic' threshold computed is shown as T. The values of the parameters m,n,Imax and Tmin are given in table 1.

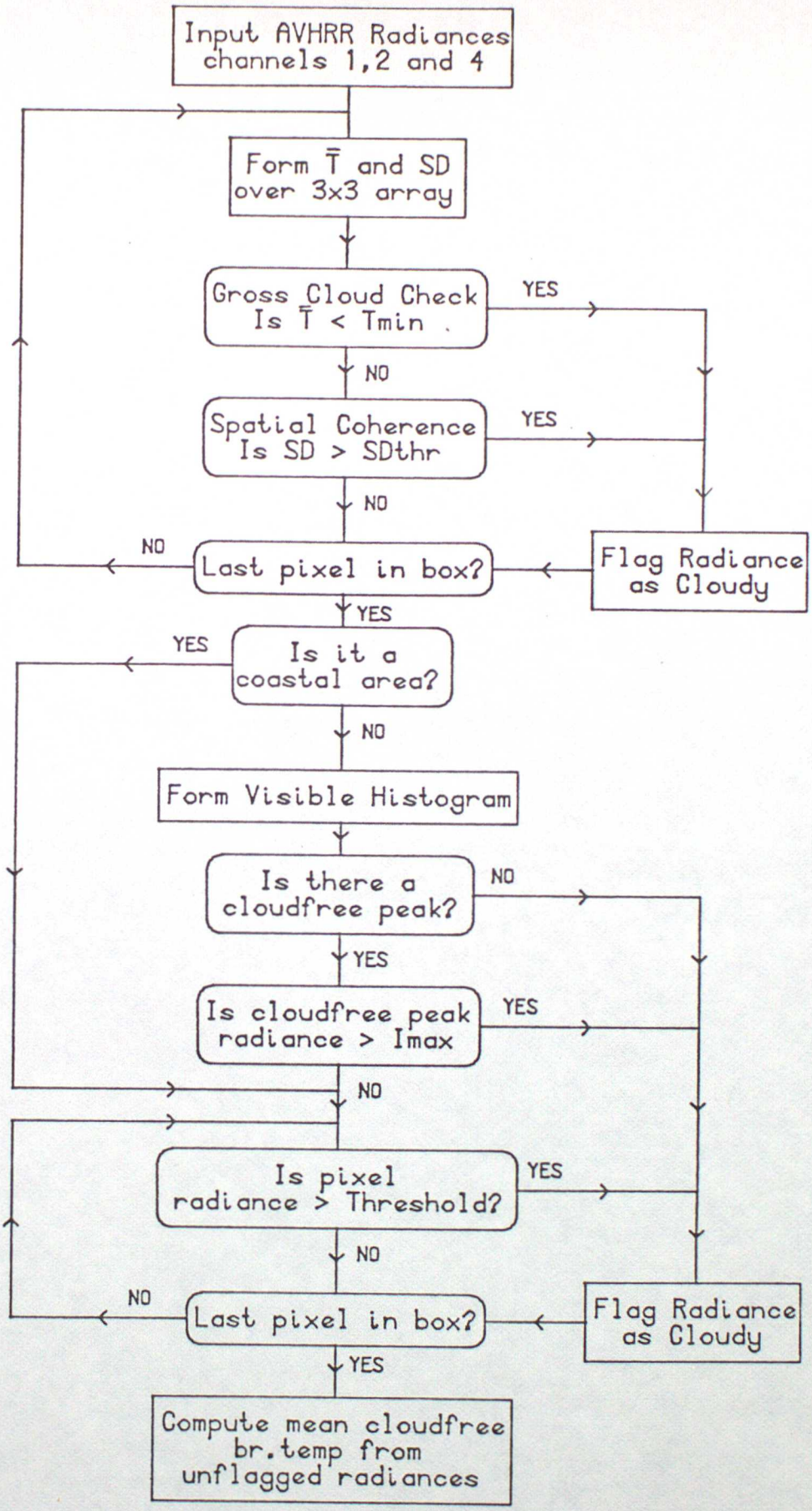

Figure 3. Outline of spatial coherence visible (SCV) algorithm for use during the day applied over a square pixel array (is box). The values for the constants Tmin, SDthr and Imax are given in table 1.

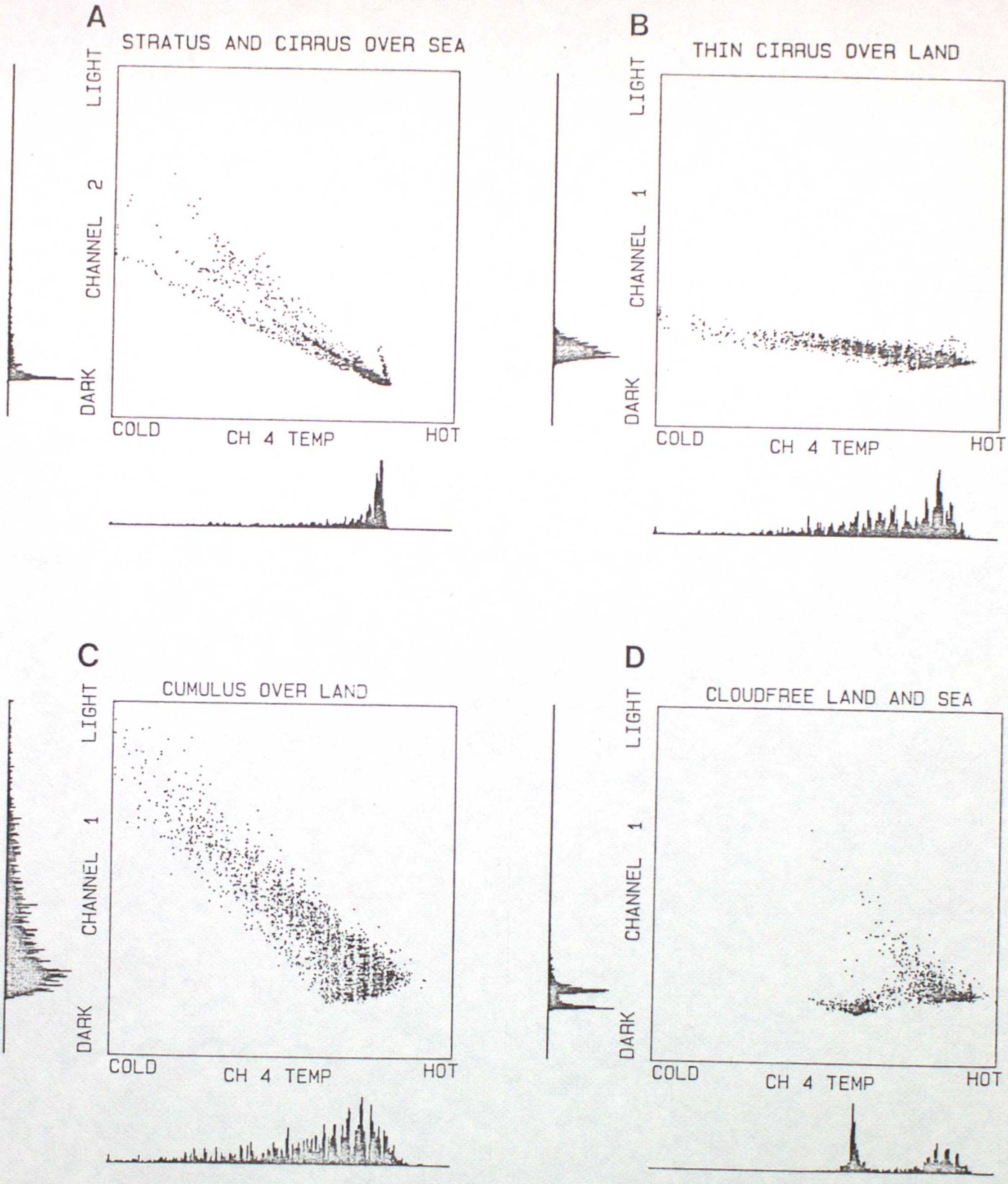

Figure 4. Bidimensional histograms of AVHRR LAC data over 50 x 50 pixel boxes for different cloud and surface types. The corresponding one dimensional histograms are also plotted.

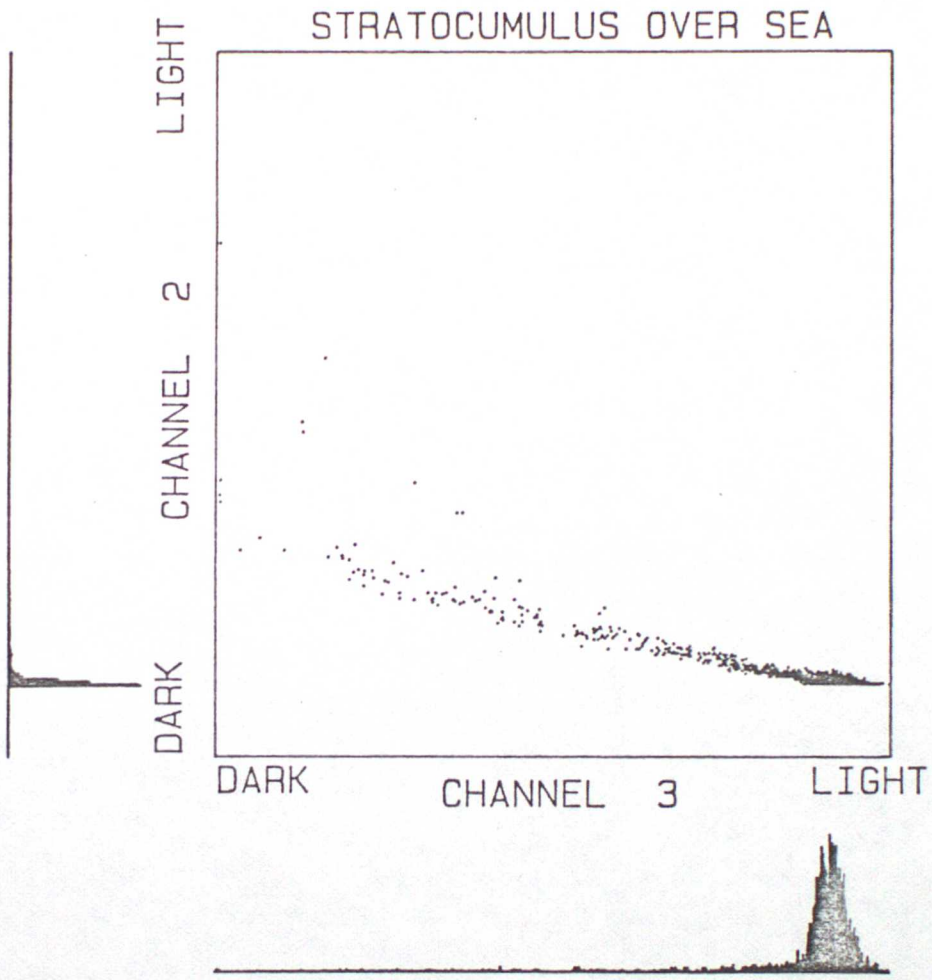

Figure 5. A bidimensional histogram of AVHRR channel 2 (0.9μm) and channel 3 (3.7μm) radiances over a 50 x 50 pixel array containing cloudfree sea surface and thin stratocumulus cloud.

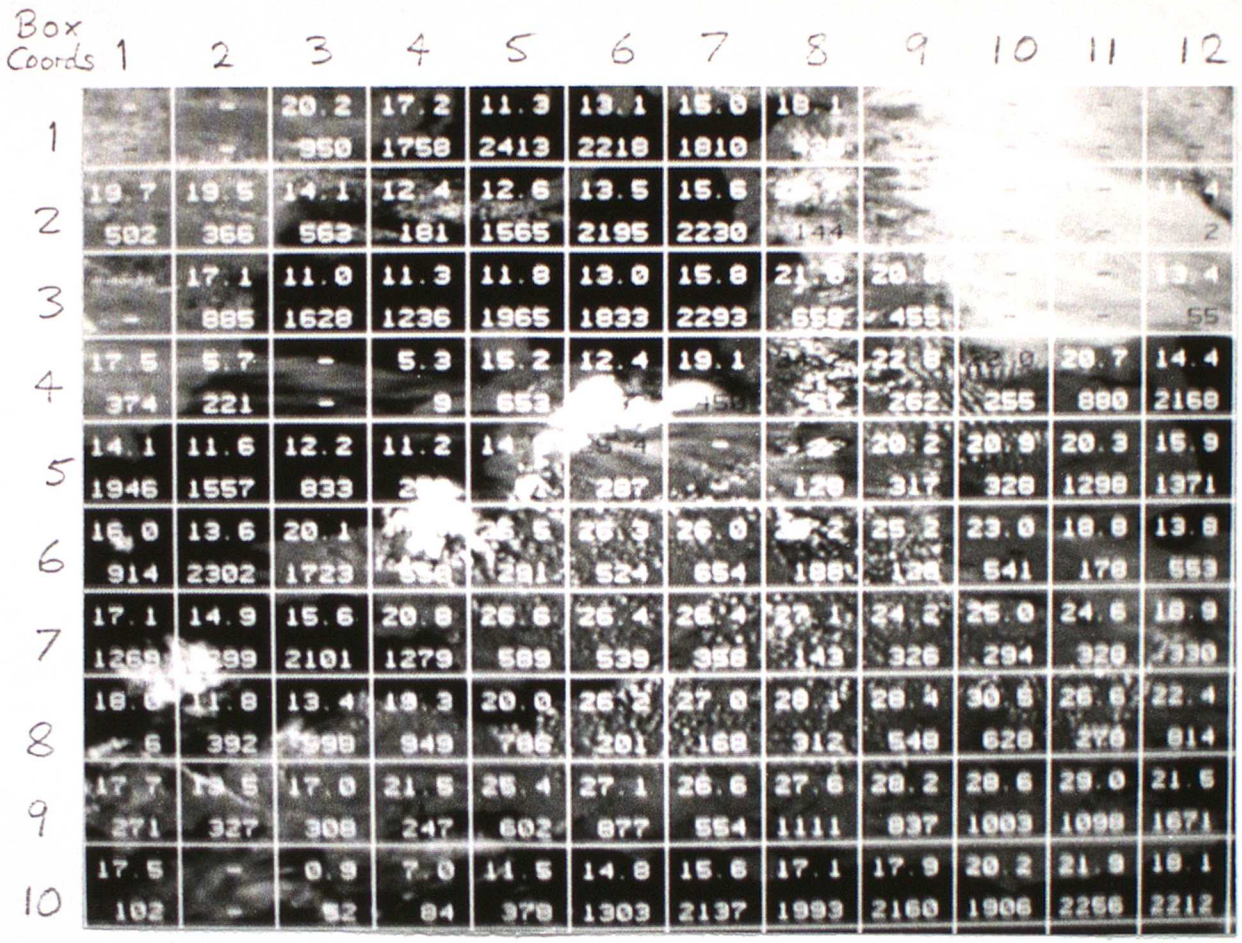

Figure 6. An AVHRR channel 2 image for 16 July 1983 at 1426gmt with boxes overlaid corresponding to those in table 2. The cloudfree brightness temperatures (C) using the SCV method together with the number of cloudfree pixels is plotted for each box. The coordinates along the edge correspond to those in table 2.

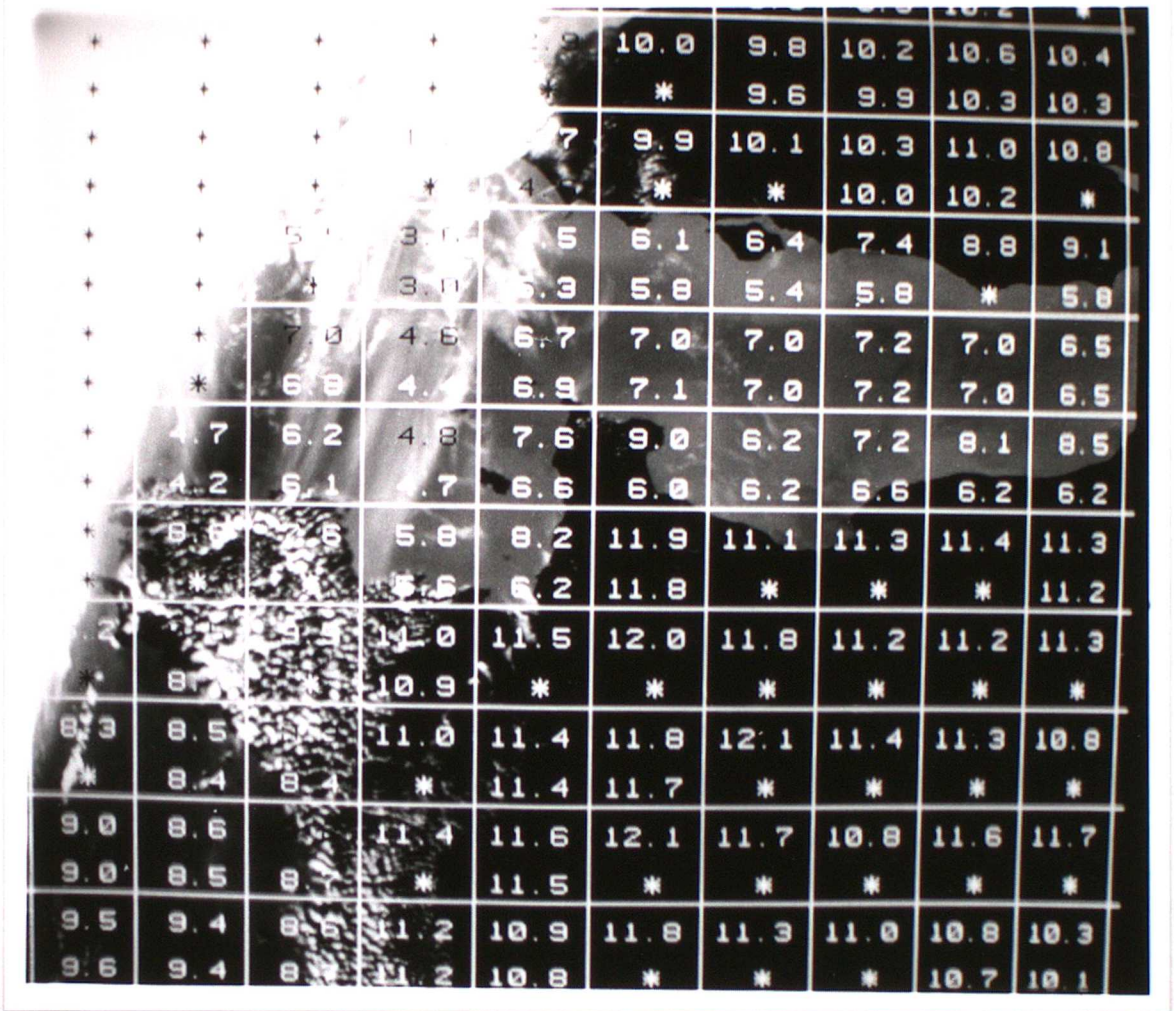

Figure 7. An AVHRR channel 4 image for 5 March 1982 at 13.37gmt. The cloudfree brightness temperatures (°C) computed using the SCV method (top) and 3.7μm radiance in place of the visible (below).